ACS APPLIED MATERIALS & INTERFACES

Research Article

www.acsami.org

Universal Strategy for Homogeneously Doping Noble Metals into Cyano-Bridged Coordination Polymers

Yu Wang,[†] Shouxin Bao,[†] Ren Li,[†] Gaozheng Zhao,[†] Zhenhua Wang,[†] Ziang Zhao,[†] and Qianwang Chen*[,†,‡]

[†]Hefei National Laboratory for Physical Sciences at the Microscale; Department of Materials Science & Engineering, University of Science and Technology of China, Hefei 230026, China

[‡]High Magnetic Field Laboratory, Hefei Institutes of Physical Science, Chinese Academy of Sciences, Hefei 230031, China

Supporting Information

ABSTRACT: Coordination polymers with large surface areas and uniform but tunable cavities have attracted extensive attention because of their unique properties and potential applications in numerous fields. The introduction of noble metal into coordination polymers, which may enhance or display new behaviors beyond their parent counterparts, presents great challenges in maintaining the fragile coordination structures and meeting the compatibility. Here, cyano-bridged coordination polymers are robust and show very nice compatibilities with a series of noble metals, such as Pd, Pt, Au, Ag. Those noble elements partially take the place of the transition metal ions under room temperature (for Au and Ag) or a mild hydrothermal environment (for Pd and Pt) without damaging the framework. By using this universal simple synthetic procedure, we prepared a series of noble metal containing metal hexacyanoferrate (MHCF) with various morphologies and structures, including Pd/Pt/Ag/Au-MnHCF, Pd/Pt/Ag/Au-CoHCF, and Pd/Pt/Ag/Au-NiHCF. Among them, Pd-MnHCF demonstrates the control of morphologies by adjusting operational details, and notably, it shows very unique, enhanced catalytic performance, reflecting the superiority of cyano-connected positive-valent Pd as a single-atom catalyst.

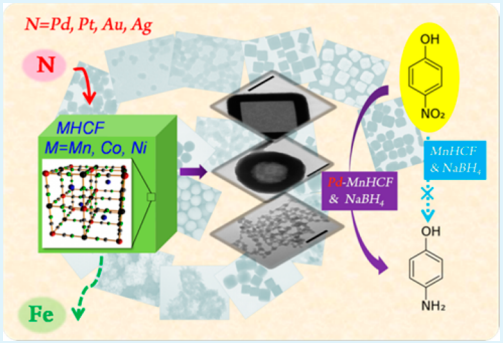

KEYWORDS: *noble metals, metal hexacyanoferrate, shape control, single-atom catalyst, Nip reduction, pseudo-zero-order kinetics*

INTRODUCTION

Coordination polymers with infinite network structures, which are constructed from metal ions as connectors and ligands as linkers, have been intensively studied and taken an important position in porous-materials area.[1−5] Coordination polymers have crystalline structures and typically are characterized by large internal surface areas, uniform but tunable cavities, and tailorable chemistry.[2,3,5] These characteristics make them very promising for a variety of applications, including gas storage,[6,7] chemical separation,[8,9] catalysis,[8,10−14] sensing,[15,16] and drug delivery.[17−21] By introducing precious metals into porous coordination polymers, it also offers opportunities to develop new type of materials that display enhanced (gas storage) or new (catalytic, optical, and electrically conductive) behaviors in comparison to the parent counterparts.[22−29]

As advanced performances could be achieved, there are many reports about the incorporation of noble metals into metal−organic frameworks (MOFs), mainly depending on two different strategies: using MOFs as templates to generate nanoparticles within their cavities[24−26,30,31] or encapsulating presynthesized nanoparticles in MOFs.[32−35] Both the two approaches are focused on zerovalent noble metals, however, the utilization efficiency of precious metals are still low when those multiatom aggregates are used for catalysis. Considering the rarity and high market price, not surprisingly, efforts to maximize the noble metal efficiency are of increasing interest. Recently, introducing positive-valent noble elements into MOFs through coordinate bonds have received intensive attention for the possibility to bridge the gap between homogeneous and heterogeneous catalysts and the intriguing single-atom catalytic performance. A gold-containing MOF, IRMOF-3-Si-Au, with a gold(III) Schiff base complex that lines the pore walls, was one of the noble-metal containing MOFs prepared by a covalent postsynthetic methodology and was reported to possess excellent activity and selectivity for alkene cyclopropanation reactions.[36] A Pd-containing MOF, with the molecular formula $[Pd(2\text{-pymo})_2]_n$, exhibited typical behaviors of heterogeneous palladium catalysts in promoting the C−C cross coupling, the aerobic oxidation, and the hydrogenation reactions.[37] However, there are limitations that the above two frameworks may not necessarily match other noble elements, and the synthesis methods are a little complicated, particularly for the covalent postsynthetic method. Moreover, their stabilities in reducing environments, surely worse than

Received: November 24, 2014
Accepted: December 30, 2014
Published: December 30, 2014

DOI: 10.1021/am508246m
ACS Appl. Mater. Interfaces 2015, 7, 2088−2096

zerovalent noble metals, are yet unknown, after all, many important catalytic reactions, such as some petroleum-related processes, take place in highly reducing environments.

Here, we demonstrate that a series of noble metals including Pd, Pt, Ag, and Au can be incorporated within crystals of readily synthesized open framework Prussian-blue type coordination polymers through a mild hydrothermal method or under room temperature without disrupting the tunable, open structures. Different from the noble-metal containing MOF prepared by covalent postsynthetic method, in which the noble elements are coordinated with functional groups grafted onto the linker, here, in the Prussian-blue type coordination compounds, the noble elements partially take the place of transition metal ions and act as framework nodes.

As previously reported, manganese hexacyanoferrate (MnHCF) using CN^- groups as linkers, transition metal Fe, and Mn ions as metallic nodes is a typical Prussian-blue analogue, showing us a general chemical formula $A_xMnFe(CN)_6{\cdot}(H_2O)_n$.[38] Unlike traditional shape-controlling methods,[21,39−41] here, through doping noble metals into MnHCF, different morphologies, including cubic nanocage, hollow sphere, and also a local area cross-linked network, can be obtained under different situations. Through repeated experiments and careful analysis, we suggest the size of the parent MnHCF crystal nucleus may be responsible for those different nanostructures. Although coordination polymers shows the potential for a variety of applications, caged, hollow, or porous coordination polymers offer a more promising approach for meeting these performance goals because the hollow interior diminishes the number of buried nonfunctional metal atoms, and their uncommon geometry provides a pathway for tailoring physical and chemical properties.[42] As an example, Pd-MnHCF shows us excellent single-atom catalytic activity on the reduction of 4-nitrophenol by $NaBH_4$ and a very rare pseudo-zero-order kinetic model, which can be attributed to the peculiarity of cyano-connected Pd. Positive-valent noble metal catalysts have commonly been underappreciated, for they may get destroyed when used in highly reducing environments.[43,44] However, the cyano-connected Pd shows us excellent resistibility and stability in the strong reducing $NaBH_4$ solution, which breaks up the monopoly of zerovalent noble metals and puts forward the possibility of using high-valent noble metal catalysts in highly reducing condition.

RESULTS AND DISCUSSION

H_2PdCl_4 was selected as the Pd source. Under mild hydrothermal conditions, MnHCF was successful transformed with H_2PdCl_4 into innovative Pd containing manganese hexacyanoferrate (marked as Pd-MnHCF). Inductively coupled plasma mass spectrometry of digested samples (dissolved in HNO_3) found a Pd:Fe:Mn mole ratio of 1:7.65:8.51. Moreover, the XP spectra confirm Pd^{2+} are connected with CN^- groups (Figure S1), suggesting that Pd^{2+} have taken the place of some Fe ions. Powder X-ray diffraction (PXRD) shows Pd-MnHCF has poorer crystallinity and smaller crystal size than its parent MnHCF (Figure 1), implying that the introduced Pd can cause tiny lattice distortion which limit the entirely replacement.

The as-prepared Pd-MnHCF cubic nanocages, hollow spheres have uniform morphology and average size of about 500 nm, shell thickness of about 80 nm (Figure 2a−d); through the close observation, all the structures are self-assembled by numerous mesocrystals, which is particularly apparent for the local area cross-linked network structure (Figure 2g and h), in

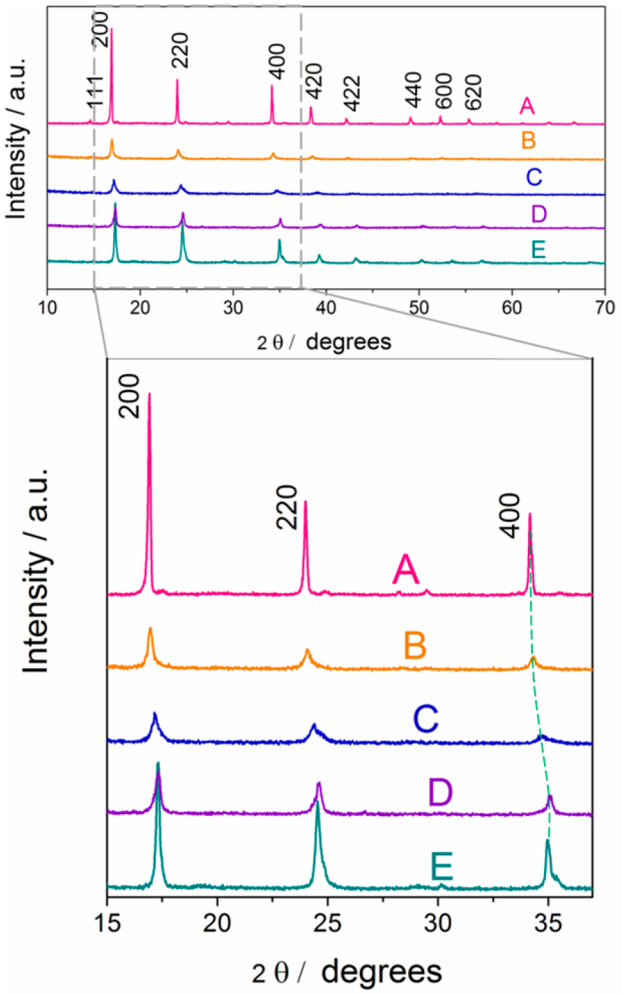

Figure 1. X-ray diffraction studies on samples of MnHCFs and Pd-MnHCFs. (A) As-prepared MnHCF synthesized at room temperature. (B) As-prepared Pd-MnHCF cubic nanocages. (C) As-prepared Pd-MnHCF hollow spheres. (D) As-prepared Pd-MnHCF local area cross-linked network structure. (E) MnHCF treated with hydrothermal reactor (MnHCF-2).

accordance with the XRD result. Although morphologies are very different between the three samples, the mild synthesis conditions in hydrothermal reactor are the same (80 °C, 5 h). The only delicate difference lies in the "right time" of adding H_2PdCl_4: cubic nanocages (Figure 2a and c) are obtained when H_2PdCl_4 is added after the mixed solution, manganese acetate and $K_3Fe(CN)_6$, has been stirred at room temperature for 20 min, at which point the suspension is seriously turbid; when the time is reduced to 10 min, the suspension is slightly turbid, and hollow spheres can be obtained (Figure 2b,d); when we change the order, adding H_2PdCl_4 into $K_3Fe(CN)_6$ solution before manganese acetate, the local area cross-linked network structure is finally obtained. In the first case, prior to adding Pd source, MnHCFs have nucleated and grown up rapidly into mature cubic nanocrystals. Relatively high temperature and pressure accelerate Pd^{2+} diffusion into the open framework and trigger an ion-exchange reaction between Fe^{2+} and Pd^{2+} while maintaining intrinsic framework structure. In contrast to other synthesis procedures for hollow nanostructures that involve corrosion induced by harsh oxidizing agents or applied potential,[45−47] the method described here proceeds through self-dissolution in water, taking advantage of the increased

DOI: 10.1021/am508246m
ACS Appl. Mater. Interfaces 2015, 7, 2088−2096

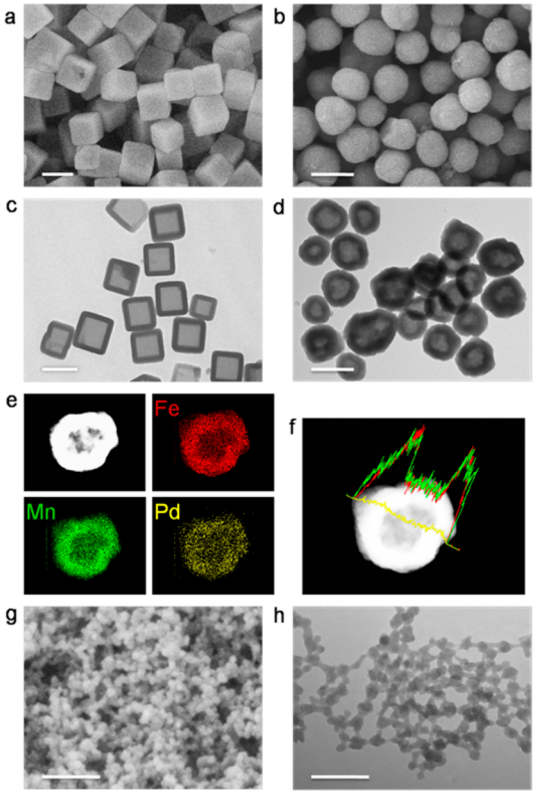

Figure 2. (a) SEM image of Pd-MnHCF cubic nanocages. (b) SEM image of Pd-MnHCF hollow spheres. (c) TEM image of Pd-MnHCF cubic nanocages. (d) TEM image of Pd-MnHCF hollow spheres. (e) HAADF-STEM image and EDX elemental mapping results for Pd-MnHCF hollow spheres, suggesting that Pd is homogeneously distributed in Pd-MnHCF hollow spheres. (f) EDS line scanning profiles of as-obtained Pd-MnHCF hollow sphere. (g) SEM image of Pd-MnHCF local area cross-linked network structure. (h) TEM image of Pd-MnHCF local area cross-linked network structure. Scale bars in parts a–d are 500 nm and in (g and h) are 200 nm.

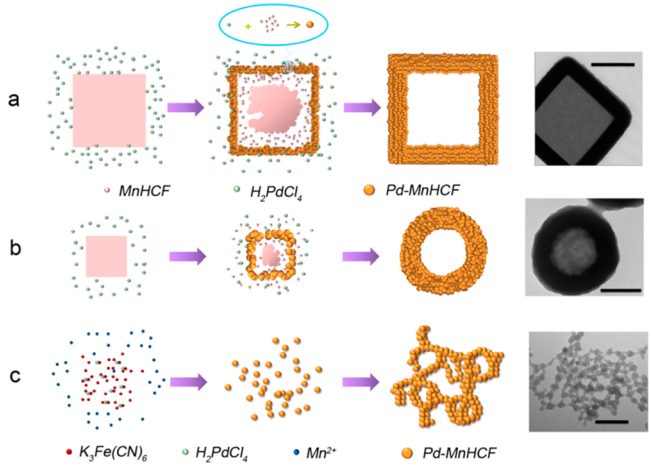

Figure 3. Schematic illustration of the evolution of the Pd-MnHCF with different morphologies in three situations and the corresponding TEM images of final samples. (a) In the first case, prior to the adding of Pd source, MnHCFs have nucleated and grown up rapidly into mature cubic nanocrystals. Pd-MnHCF cubic nanocages are finally obtained. (b) In the second case, H_2PdCl_4 is added at the point when MnHCFs have already nucleated but do not have time to grow up into enough size. Pd-MnHCF hollow spheres are finally obtained. (c) In the third case, Fe-CN-Pd molecules are first formed, and Mn^{2+} ions are added 10 min later. There finally formed the local area cross-linked network structure. All the scale bars are 200 nm.

solubility under higher temperature and higher acidity. Doping with Pd initially happens at outermost layer of MnHCF, and stabilizes the shell, as the reaction proceeds, the inner space of MnHCF gradually disintegrates, forming hollow structure, meanwhile the released MnHCF molecules or nanoclusters migrate to the cube surfaces and are captured by $PdCl_4^{2-}$, generating Pd-MnHCF mesocrystals that grow on the shell. At last, there form the as-prepared cubic nanocages (as showed in Figure 3a).

Samples at three representative stages (0, 2.5, and 5 h) were examined by transmission electron microscopy (TEM) (Figure S2b–d). The initial solid nanostructures gradually eroded into hollow frames, and the bulk composition changed from MnHCF to MnHCF/Pd-MnHCF coexistence and eventually Pd-MnHCF, as evidenced by XRD patterns (Figure S2a): All three samples were face-centered cubic (fcc), and the three main XRD peaks of the intermediate sample—(200), (220), and (400)—split into two groups of subpeaks located near those of MnHCF and Pd-MnHCF respectively; during the evolution process, the peaks shifted toward higher angle (decreased d spacing), implying that the nanostructures had changed from MnHCF to Pd-MnHCF.

In the second case, H_2PdCl_4 is added at the point when MnHCFs have already nucleated but do not have time to grow up into enough size. After the outermost layer has been transformed into Pd-MnHCF, along with the disintegrating of inner space, the shell layer is covered by layer upon layer of Pd-MnHCF mesocrystals, as they are self-assembled following principle of minimizing the surface energy,[48] there eventually form the hollow spheres (Figure 3b). Both EDS line scanning profiles and mapping images (Figure 2e and f) demonstrate the homogeneous distribution of Pd, Fe, and Mn.

In the third case, Fe-CN-Pd molecules are first formed at room temperature, but no precipitates come into being even after Mn^{2+} has been added. However, in the following Mn^{2+}-rich hydrothermal environment, partial Fe ions are displaced by Pd, and Mn get involved in the crystallization simultaneously. Because of the lattice deformation caused by Pd doping, no cubic structure forms, but those small mesocrystals tend to oriented growth, connect with each other,[46] and form the local area cross-linked network structure (Figure 3c), similar to that of NiHCF.[48,49]

X-ray diffraction studies on samples of MnHCF before and after the hydrothermal treatment (80 °C, 5 h) without the disturbance of Pd are helpful for understanding the phase transition process (Figure 1A and E). Different from the as-prepared MnHCF synthesized at room temperature, after treatment in hydrothermal reactor, the new MnHCF (marked as MnHCF-2) manifest an apparent lattice transition. X-ray diffraction patterns for the as-made MnHCF (Figure 1A) shows nine resolved peaks with d spacings of 6.09, 5.24, 3.70, 2.61, 2.34, 2.15, 1.85, 1.75, and 1.66 Å. These peaks display d-value ratios of $\sqrt{3}:\sqrt{4}:\sqrt{8}:\sqrt{16}:\sqrt{20}:\sqrt{24}:\sqrt{32}:\sqrt{36}:\sqrt{40}$, which are indexable as (111), (200), (220), (400), (420), (422), (440), (600), and (620) reflections, respectively, in the face-centered cubic structure (a = 10.48 Å). After hydrothermal treatment of the sample at 80 °C, those XRD peaks (Figure 1E) are observed with decreased d spacings of 5.89, 5.12, 3.62, 2.56, 2.29, 2.09, 1.81, 1.70, and 1.62 Å (ratios $\sqrt{3}:\sqrt{4}:\sqrt{8}:\sqrt{16}:\sqrt{20}:\sqrt{24}:\sqrt{32}:\sqrt{36}:\sqrt{40}$), which also can be indexable

DOI: 10.1021/am508246m
ACS Appl. Mater. Interfaces 2015, 7, 2088–2096

as (111), (200), (220), (400), (420), (422), (440), (600), and (620) reflections of the face-centered cubic structure, but the lattice constant (a = 10.23 Å) is obviously smaller.

As Pd get involved, the above phase transition process is effectively prevented, as demonstrated by XRD results (Figure 1): All samples in the above three cases are face-centered cubic (fcc), and the main XRD peaks for each sample—such as (200), (220), and (400)—are located between those of as-prepared MnHCF and MnHCF-2; from the first case to the third, the peaks shift toward higher angle (decreased d spacing), which suggests that when MnHCFs have nucleated and grown up rapidly into mature cubic nanocrystals (case one), the added Pd penetrates into MnHCF, taking the place of Fe, not only does not disrupt the lattice but stabilizes it, leading to a lattice structure similar to that of MnHCF (Figure 1A and B); when MnHCFs have already nucleated but do not have time to mature (case two), though Pd dopants do the best to stabilize, there is larger lattice change (Figure 1C); and in case three, Pd-MnHCF-2 forms directly, showing similar lattice to MnHCF-2 (Figure 1D and E).

The catalytic reduction of 4-nitrophenol (Nip) by $NaBH_4$ to 4-aminophenol was chosen as a model reaction to evaluate the catalytic ability of the synthesized Pd-MnHCF cubic nanocages, and UV−vis spectroscopy was used to monitor its kinetics. The complete catalytic reaction could be visually appreciated by the color change of the solution: the reduction reaction did not proceed without catalyst, as evidenced by a constant original bright yellow, corresponding to an absorption peak at 400 nm; when Pd-MnHCF catalyst was introduced, the solution rapidly turned colorless, and the absorption at 400 nm quickly decreased and absorption at 300 nm increased accordingly (Figure 4a).

Interestingly, indicating pseudo-zero-order kinetics, the absorbance intensity of the UV−vis spectroscopy changes linearly with time (Figure 4b), different from almost all the previously reported pseudo-first-order kinetic metal nanoparticle catalysts. Though the rate constants in different kinetic models are very different, Pd-MnHCF's superior performance than the reported Pd nanoparticles with mean diameter at 2.85 nm still can be known by comparing Pd consumptions and corresponding reaction rates.[50] Generally, the utilization efficiency of noble-metal in conventional supported catalysts is far less than satisfactory, for their way of beings are zerovalent multiatom aggregates, from original bulk materials to fashionable nanoparticles and atomic clusters; even as small as 2 nm, still about half the particle atoms are buried.[51−54] Some of Pd-MnHCF's excellent catalytic activity may be traceable to, unlike conventional noble metal particles, the uniform distribution of Pd atoms throughout the open framework structure, which could offer numerous adsorption sites for other reactants, with the result that nearly all the Pd atoms sufficiently get involved in the catalytic process.

In addition to the unique pseudo-zero-order kinetics, we also found some other unexpected interesting phenomena, which may be helpful to speculate the catalytic reaction process. Figure 5a depicted the time dependences of the absorption peak of Nip at 400 nm under different catalyst consumptions; it shows, against most reported catalytic reaction and the general consensus, that the larger catalyst dosage not only does not improve reaction rate, but decrease in trend: with the same dosage of $NaBH_4$ and Nip, the reaction rate is larger at a catalyst consumption of 50 μL, is moderate and almost the same at 100, 150, 200 μL, and is smaller at 300 μL. To further

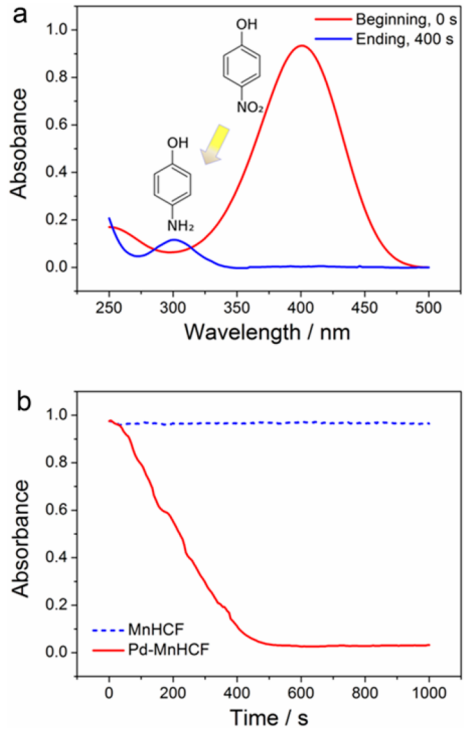

Figure 4. Catalytic performance. (a) UV−vis absorption spectra for the reduction of Nip catalyzed by Pd-MnHCF cubic nanocages. (b) Time dependence of the absorption of Nip at 400 nm. Pure MnHCF shows no catalytic activity, while Pd-MnHCF shows excellent catalytic activity, and very rare pseudo-zero-order kinetics. The dosages of Pd-MnHCF, Nip, and $NaBH_4$ are 100, 50, and 200 μL, respectively.

investigate, using constant dosage of Nip and catalyst, we observe the reaction rate increases with the larger $NaBH_4$ consumption (Figure 5b); however, rate constants are neither the fit of usual Langmuir−Hinshelwood (LH) model,[55,56] nor proportional to $NaBH_4$ dosage, they slightly shift from the direct proportion line (the red dotted line): rate constant shift upward at a $NaBH_4$ dosage of 400 μL, downward at 100 μL (Figure 5c). Apparently, $NaBH_4$ plays a more eye-catching role than the so-called catalyst in the process. Rather than the pure Pd-MnHCF acting as catalyst, it is better to say the combination of Pd-MnHCF and $NaBH_4$ activate the catalytic reaction. In other words, Pd-MnHCF is first triggered by $NaBH_4$, then the activated catalyst stimulate the reduction of Nip. As depicted in Figure 5a, for the constant dosages of $NaBH_4$, though catalyst dosage increases obviously (from 100 to 200 μL), the amount of active-sites in Pd-MnHCF keeps constant, with the result that the reaction rates remain unchanged. When Pd-MnHCF is increased to 300 μL, the total active-sites even decrease, for the increased dosage of Pd-MnHCF dilutes, and weakens the activating ability of $NaBH_4$, in accordance with, in Figure 5c, the lower rate constant below the red dotted line under a condition of relative more Pd-MnHCF, but less $NaBH_4$. When Pd-MnHCF is decreased to 50 μL, some active sites are excessively activated, implying some zerovalent Pd, which can be proved by the XPS results, are irreversibly formed (Figure S3). With the combined action of the active sites and zerovalent Pd, it showed an absorbance−time curve between the zero-order and first-order kinetic models and an improved reaction rate corresponding to, in Figure 5c, the higher rate constant above the red dotted line under a condition of relative less Pd-MnHCF but more $NaBH_4$.

DOI: 10.1021/am508246m
ACS Appl. Mater. Interfaces 2015, 7, 2088−2096

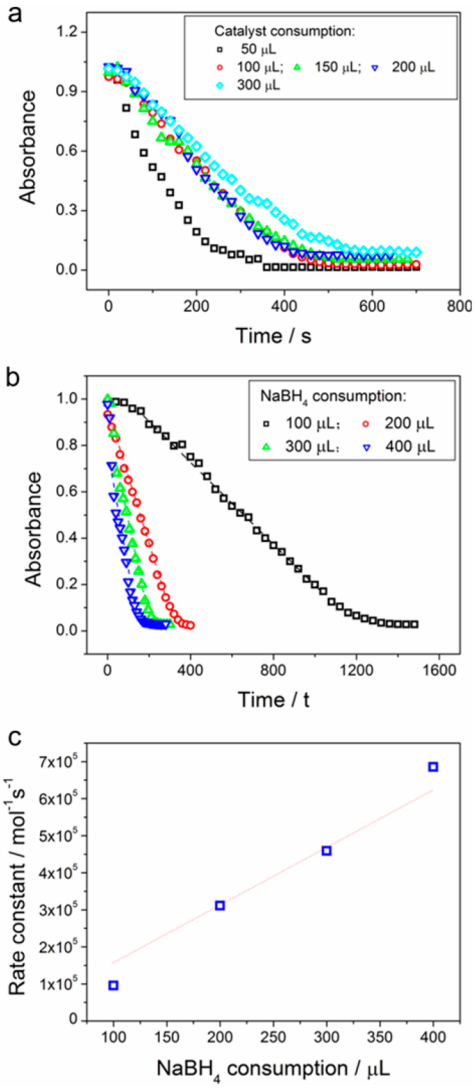

Figure 5. Catalytic performance of Pd-MnHCF cubic nanocages. (a) Time dependences of the absorption peak of Nip at 400 nm under different catalyst consumptions. The dosage of Nip is 50 μL, and $NaBH_4$ is 200 μL. (b) Time dependences of the absorption peak of Nip at 400 nm under different $NaBH_4$ consumptions. The dosage of Nip is 50 μL, and Pd-MnHCF is 100 μL. (c) Dependence of the kinetic constant on the $NaBH_4$ consumption, corresponding to part b. The red dotted line is a direct proportion line which is based on the assumption: when $NaBH_4$ consumption doubles, kinetic constant doubles.

The above viewpoint is also reasonable in comprehending the pseudo-zero-order kinetic model, namely reaction rate keeps constant ignoring the gradually decreased reactant concentration. Generally, in solution, Nips adsorb on Pd-MnHCF and then partially get desorbed into water, eventually reaching equilibrium. In most cases (traditional using noble metal particles as catalysts), active sites are relatively much richer, so the adsorption rate is the rate-determining step, and reaction rate seriously depends on the reactant concentration, leading to pseudo-first-order kinetics.[50,55,56] However, here, it is reasonable to believe the adsorption of Nip is fast enough, for, as depicted in Figure 5, commonly reported "induction time t_0" is almost unseen,[55,57,58] and Nips get reduced as soon as we add in the catalyst, so rather than Nip concentration, but the created, transient active-sites in Pd-MnHCF determine the reaction rate, resulting in the pseudozero-order kinetics.[58] Figure 6 describes the catalytic procedure of this reaction. After

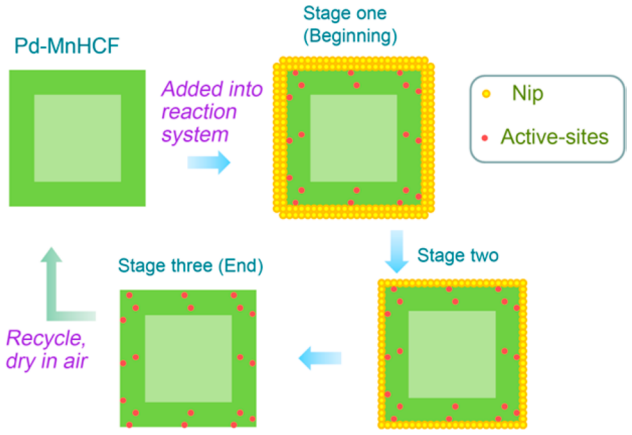

Figure 6. Catalytic outline for the reduction of 4-nitrophenol (Nip) by $NaBH_4$ using Pd-MnHCF cubic nanocages as catalysts. As the adsorption of Nip is much faster than its desorption, the number of active-sites in Pd-MnHCF determined the reaction rate, resulting in pseudo-zero-order kinetics. After completing the reaction, and being dried in air, the chemical environment of Pd in the recycled catalyst fully recovers, as the XPS result presented (in Figure S3).

completing the reaction, and being dried in air, the chemical environment of Pd in the recycled catalyst fully recovers, as the XPS result presented (Figure S3). It is worth noting that those active-sites are not constant, at the moment Pd-MnHCFs get an electron from $NaBH_4$, they instantly give it to Nip, and return to the original condition, the following active-sites may be created elsewhere, repeating the process of their predecessors.

Encouraged by the success of incorporating Pd into MnHCF and controlling the formation of different morphologies and nanostructrues, the doping strategy was extended to synthesize Pt-MnHCF, Ag-MnHCF, Au-MnHCF, Pd-CoHCF, Pt-CoHCF, Ag-CoHCF, Au-CoHCF, Pd-NiHCF, Pt-NiHCF, Ag-NiHCF, and Au-NiHCF, whose basic sizes and morphologies were also determined by their parent metal hexacyanoferrates. Similar to that of Pd-MnHCF, the doping of Pt need to be triggered by high temperature and stress in hydrothermal environment. Moreover, cubic structure and sphere can also be obtained by controlling the timing of adding Pt source, though the hollow structures are not that obvious (Figure S4b and d). Even more convenient than the doping of Pd and Pt, the ion-exchange reactions between Fe^{2+} and Ag^+ or Au^+ can take place at room temperature. With the relative high solubility of MnHCF in water, which benefits the formation of hollow structure in Pd-MnHCF, collecting completely cubic structure of MnHCF seems impossible (Figure S2b). And the adding Ag could act as the fixactive which record the growth of MnHCF (Figure S5), by contrast, the adding of Au slightly stretched the mesocrysitals (Figure S4g and h). X-ray diffraction studies on samples of Ag-MnHCF and Au-MnHCF demonstrate that the adding of Ag or Au alters the backbones of the framework structure (Figure S6), while Pt, like Pd, just causes a slight lattice distortion. Adding Ag creates a new phase (Figure S6), and the new three strong peaks can be aligned to AgCN (JCPDS 89-0927), indicating that silver tends to replace not only Fe but also Mn. A very interesting phenomenon happens by introducing Au into the framework: while the peaks aligned

DOI: 10.1021/am508246m
ACS Appl. Mater. Interfaces 2015, 7, 2088−2096

to (220), (420), (422), (440), and (620) face split into two subpeaks, peaks aligned to (200), (400), and (600) remain intact; it is also obvious for Au-CoHCF (Figure 7a). The most

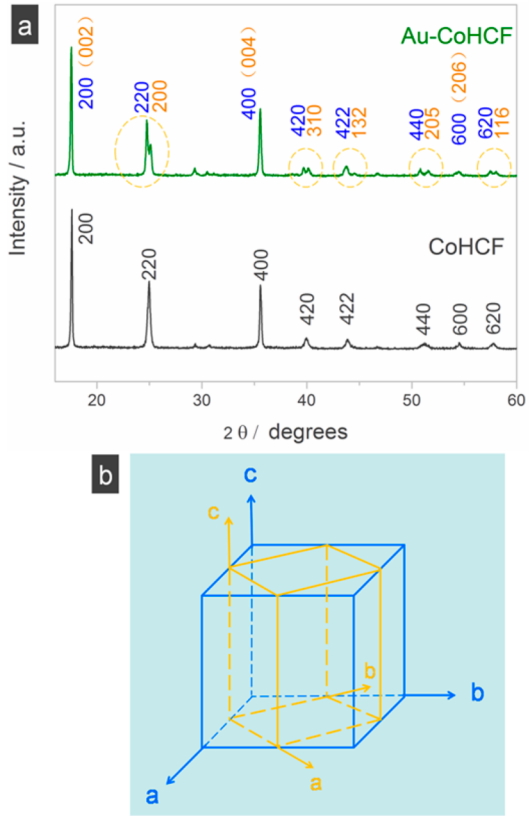

Figure 7. (a) XRD patterns of CoHCF and Au-CoHCF and (b) sketch for lattice transformation from cubic system (blue) to tetragonal system (orange). Similar to that of Au-MnHCF, while the peaks which can be aligned to (220), (420), (422), (440), and (620) face split into two subpeaks, peaks aligned to (200), (400), and (600) remain intact.

reasonable explanation is that Au disrupt the order of Fe and Mn, from ordered Fe−C≡N−Mn to disordered (Fe,Mn,Au)−C≡N−(Fe,Mn,Au), causing a reduced structural symmetry. A smaller coaxial unit cell with tetragonal structure forms inside the original cubic unit cell, creating some diffraction peaks almost overlapped with that former cubic unit cell and some new peaks alongside (Figure 7b).

Because the supersaturation in our experiments showed an increase order of MnHCF< CoHCF< NiHCF, with the same molality, the three displayed different critical particle sizes in reverse order, in accordance with the equation: $r_c = 2\Omega\gamma_{cf}/kT\ln(1+\sigma)$.[59] Here γ_{cf} denotes the specific interfacial free energy between the crystal and the mother phase; Ω is the volume of growth units; and σ is supersaturation. As shown in Figure 8 and Figure S7, noble-metal containing NiHCFs are also much smaller than noble-metal containing CoHCFs, and though noble metals do not changed the basic sizes and morphologies of both CoHCF and NiHCF, there are some small differences: as both Pd and Pt were introduced through the hydrothermal treatment, the surface of Pd/Pt containing NiHCF or CoHCF are not as smooth as that of Au/Ag containing metal hexacyanoferrates; the morphologies of Au-CoHCF and Au-NiHCF are almost the same as that of CoHCF and NiHCF; however, different from the other three noble

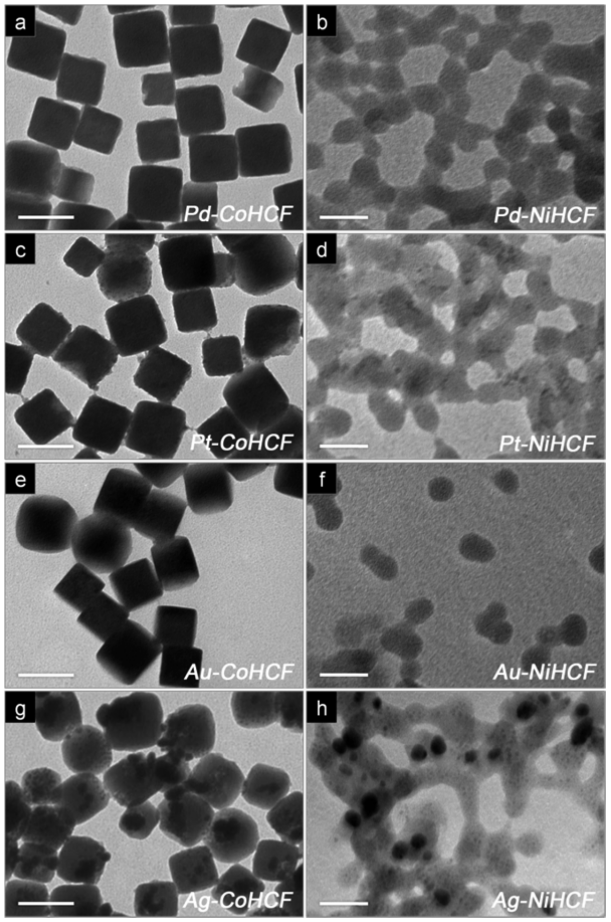

Figure 8. Morphology and structure studies on samples of Pd/Pt/Au/Ag-CoHCF and Pd/Pt/Au/Ag-NiHCF. (a) SEM image of as-prepared Pd-CoHCF. (b) TEM image of as-prepared Pd-NiHCF. (c) SEM image of as-prepared Pt-CoHCF. (d) TEM image of as-prepared Pt-NiHCF. (e) SEM image of as-prepared Au-CoHCF. (f) TEM image of as-prepared Au-NiHCF. (g) SEM image of as-prepared Ag-CoHCF. (h) TEM image of as-prepared Ag-NiHCF. Scale bars in a, c, e, and g are 200 nm, and in b, d, f, and h, they are 50 nm.

metals, Ag ions in the metel hexacyanoferrates seem to have much stronger attractions between each other, for they tend to aggregate and show higher contrast in the whole particles (Figure 8g and h). Figure S9a shows the X-ray diffraction patterns of Pd/Pt/Au/Ag-CoHCF and CoHCF: in comparison with CoHCF, Pd/Pt/Ag-CoHCF show the similar lattices with slightly different lattice constants, while some diffraction peaks of Au-CoHCF split like that of Au-MnHCF. Also the adding of Au generates a smaller coaxial unit cell which has tetragonal structure inside the former cubic CoHCF unit cell, and main peaks are indexable (Figure 7a). Figure S9b shows the X-ray diffraction patterns of Pd/Pt/Au/Ag-NiHCF and NiHCF: in comparison with NiHCF, Pd/Pt/Au-NiHCF show the similar lattices with slightly different lattice constants, while an extra diffraction peak of Ag-NiHCF emerges, and it can be aligned to the (110) face of AgCN (JCPDS 89-0927).

The above noble metal containing metal hexacyanoferrate are supposed to play important roles in plentiful areas. Among them, Pd-MnHCF has shown excellent, very unique catalytic performance in the reduction of 4-nitrophenol and outstanding resistibility and stability in the strong reducing $NaBH_4$ solution, breaking up the monopoly of zerovalent noble metals. Also, our

DOI: 10.1021/am508246m
ACS Appl. Mater. Interfaces 2015, 7, 2088−2096

recent experiments implied the improved OER activity through doping Pt into $Co_3[Co(CN)_6]_2$. Furthermore, Pd containing metal hexacyanoferrate is also promising in hydrogen storage, for the reported dehydrated Prussian-blue analogues have showed high hydrogen storage,[60,61] and experiments have demonstrated that the adding of Pd into MOF can usually enhance the gas adsorption property.[26,62]

CONCLUSIONS

In summary, through careful experimental studies, we have demonstrated that a variety of noble elements, including Pd, Pt, Au, and Ag, can sneak deep into the preprepared metel hexacyanoferrate and successfully take the place of some iron ions through a solution-mediated reaction. The whole process is operated through a mild hydrothermal method or under room temperature without disrupting the tunable, open framework structures. In addition to the good compatibility of Prussian-blue type coordination polymers to access a series of noble metals and the convenient, mild approach, various aspects of nanostructure (e.g., size, morphology, and hollow structure formation) can be influenced by controlling critical aspects of the metal hexacyanoferrates precursors. The diversity in noble elements, and their uniform distribution throughout the open framework structure, together with highly controllable nanostructures will no doubt help to access a wide range of high performances, especially in areas of highly stable single-atom catalysis, gas storage. Along with introducing a series of noble elements mentioned above, this doping strategy also shows potential of bringing in a broad range of rare earth elements, which may help to make efficient T1 and T2 contrast agents for MRI.

ASSOCIATED CONTENT

Supporting Information

Full experimental details, additional electron microscopic images, XRD patterns, XP spectra, scheme of the catalytic procedure. This material is available free of charge via the Internet at http://pubs.acs.org.

AUTHOR INFORMATION

Corresponding Author

*E-mail: cqw@ustc.edu.cn.

Notes

The authors declare no competing financial interest.

ACKNOWLEDGMENTS

This work was supported by the National Natural Science Foundation (NSFC, 21271163, U1232211). We thank Prof. Zhou Gui'en for constructive discussions on the analysis of XRD patterns about Au-MnHCF and Au-CoHCF and Zhang Peng for his helpful suggestion about the catalytic study.

REFERENCES

(1) Abrahams, B. F.; Hoskins, B. F.; Michail, D. M.; Robson, R. Assembly of Porphyrin Building Blocks into Network Structures with Large Channels. *Nature* **1994**, *369*, 727−729.

(2) Li, H.; Eddaoudi, M.; O'Keeffe, M.; Yaghi, O. M. Design and Synthesis of an Exceptionally Stable and Highly Porous Metal-organic Framework. *Nature* **1999**, *402*, 276−279.

(3) Yaghi, O. M.; O'Keeffe, M.; Ockwig, N. W.; Chae, H. K.; Eddaoudi, M.; Kim, J. Reticular Synthesis and the Design of New Materials. *Nature* **2003**, *423*, 705−714.

(4) Lee, S.; Mallik, A. B.; Xu, Z.; Lobkovsky, E. B.; Tran, L. Small Amphiphilic Organics, Coordination Extended Solids, and Constant Curvature Structures. *Acc. Chem. Res.* **2005**, *38*, 251−261.

(5) Tranchemontagne, D. J.; Mendoza-Cortés, J. L.; O'Keeffe, M.; Yaghi, O. M. Secondary Building Units, Nets and Bonding in the Chemistry of Metal−organic Frameworks. *Chem. Soc. Rev.* **2009**, *38*, 1257−1283.

(6) Wong-Foy, A. G.; Matzger, A. J.; Yaghi, O. M. Exceptional H_2 Saturation Uptake in Microporous Metal-organic Frameworks. *J. Am. Chem. Soc.* **2006**, *128*, 3494−3495.

(7) Britt, D.; Furukawa, H.; Wang, B.; Glover, T. G.; Yaghi, O. M. Highly Efficient Separation of Carbon Dioxide by a Metal-organic Framework Replete with Open Metal Sites. *Proc. Nati. Acad. Sci.* **2009**, *106*, 20637−20640.

(8) Seo, J. S.; Whang, D.; Lee, H.; Im Jun, S.; Oh, J.; Jeon, Y. J.; Kim, K. A Homochiral Metal−organic Porous Material for Enantioselective Separation and Catalysis. *Nature* **2000**, *404*, 982−986.

(9) Chen, B.; Liang, C.; Yang, J.; Contreras, D. S.; Clancy, Y. L.; Lobkovsky, E. B.; Yaghi, O. M.; Dai, S. A Microporous Metal−Organic Framework for Gas-Chromatographic Separation of Alkanes. *Angew. Chem.* **2006**, *118*, 1418−1421.

(10) Tanabe, K. K.; Cohen, S. M. Engineering a Metal−Organic Framework Catalyst by Using Postsynthetic Modification. *Angew. Chem.* **2009**, *121*, 7560−7563.

(11) Corma, A.; Garcia, H.; Llabrés i Xamena, F. Engineering Metal Organic Frameworks for Heterogeneous Catalysis. *Chem. Rev.* **2010**, *110*, 4606−4655.

(12) Vermoortele, F.; Ameloot, R.; Vimont, A.; Serre, C.; De Vos, D. An Amino-modified Zr-terephthalate Metal−organic Framework as an Acid−base Catalyst for Cross-aldol Condensation. *Chem. Commun.* **2011**, *47*, 1521−1523.

(13) Yoon, M.; Srirambalaji, R.; Kim, K. Homochiral Metal−organic Frameworks for Asymmetric Heterogeneous Catalysis. *Chem. Rev.* **2011**, *112*, 1196−1231.

(14) Zhang, Z.; Chen, Y.; He, S.; Zhang, J.; Xu, X.; Yang, Y.; Nosheen, F.; Saleem, F.; He, W.; Wang, X. Hierarchical Zn/Ni-MOF-2 Nanosheet-Assembled Hollow Nanocubes for Multicomponent Catalytic Reactions. *Angew. Chem.* **2014**, *126*, 12725−12729.

(15) Chen, B.; Wang, L.; Xiao, Y.; Fronczek, F. R.; Xue, M.; Cui, Y.; Qian, G. A Luminescent Metal−organic Framework with Lewis Basic Pyridyl Sites for the Sensing of Metal Ions. *Angew. Chem., Int. Ed.* **2009**, *48*, 500−503.

(16) Jiang, H.-L.; Tatsu, Y.; Lu, Z.-H.; Xu, Q. Non-, Micro-, and Mesoporous Metal− organic Framework Isomers: Reversible Transformation, Fluorescence Sensing, and Large Molecule Separation. *J. Am. Chem. Soc.* **2010**, *132*, 5586−5587.

(17) Horcajada, P.; Chalati, T.; Serre, C.; Gillet, B.; Sebrie, C.; Baati, T.; Eubank, J. F.; Heurtaux, D.; Clayette, P.; Kreuz, C. Porous Metal-organic-framework Nanoscale Carriers as a Potential Platform for Drug Delivery and Imaging. *Nat. Mater.* **2010**, *9*, 172−178.

(18) Imaz, I.; Rubio-Martínez, M.; García-Fernández, L.; García, F.; Ruiz-Molina, D.; Hernando, J.; Puntes, V.; Maspoch, D. Coordination Polymer Particles as Potential Drug Delivery Systems. *Chem. Commun.* **2010**, *46*, 4737−4739.

(19) Sun, C. Y.; Qin, C.; Wang, C. G.; Su, Z. M.; Wang, S.; Wang, X. L.; Yang, G. S.; Shao, K. Z.; Lan, Y. Q.; Wang, E. B. Chiral Nanoporous Metal-organic Frameworks with High Porosity as Materials for Drug Delivery. *Adv. Mater.* **2011**, *23*, 5629−5632.

(20) Qin, J.-S.; Du, D.-Y.; Li, W.-L.; Zhang, J.-P.; Li, S.-L.; Su, Z.-M.; Wang, X.-L.; Xu, Q.; Shao, K.-Z.; Lan, Y.-Q. N-rich Zeolite-like Metal−organic Framework with Sodalite Topology: High CO_2 Uptake, Selective Gas Adsorption and Efficient Drug Delivery. *Chem. Sci.* **2012**, *3*, 2114−2118.

(21) Lian, H.-Y.; Hu, M.; Liu, C.-H.; Yamauchi, Y.; Wu, K. C.-W. Highly Biocompatible, Hollow Coordination Polymer Nanoparticles as Cisplatin Carriers for Efficient Intracellular Drug Delivery. *Chem. Commun.* **2012**, *48*, 5151−5153.

(22) Szeto, K. C.; Prestipino, C.; Lamberti, C.; Zecchina, A.; Bordiga, S.; Bjørgen, M.; Tilset, M.; Lillerud, K. P. Characterization of a New

DOI: 10.1021/am508246m
ACS Appl. Mater. Interfaces 2015, 7, 2088−2096

Porous Pt-containing Metal-organic Framework Containing Potentially Catalytically Active Sites: Local Electronic Structure at the Metal Centers. *Chem. Mater.* **2007**, *19*, 211−220.
(23) Wang, C.; deKrafft, K. E.; Lin, W. Pt Nanoparticles@ Photoactive Metal−organic Frameworks: Efficient Hydrogen Evolution via Synergistic Photoexcitation and Electron Injection. *J. Am. Chem. Soc.* **2012**, *134*, 7211−7214.
(24) Sabo, M.; Henschel, A.; Fröde, H.; Klemm, E.; Kaskel, S. Solution Infiltration of Palladium into MOF-5: Synthesis, Physisorption and Catalytic Properties. *J. Mater. Chem.* **2007**, *17*, 3827−3832.
(25) Hermes, S.; Schröter, M. K.; Schmid, R.; Khodeir, L.; Muhler, M.; Tissler, A.; Fischer, R. W.; Fischer, R. A. Metal@MOF: Loading of Highly Porous Coordination Polymers Host Lattices by Metal Organic Chemical Vapor Deposition. *Angew. Chem., Int. Ed.* **2005**, *44*, 6237−6241.
(26) Zlotea, C.; Campesi, R.; Cuevas, F.; Leroy, E.; Dibandjo, P.; Volkringer, C.; Loiseau, T.; Férey, G.; Latroche, M. Pd Nanoparticles Embedded into a Metal-organic Framework: Synthesis, Structural Characteristics, and Hydrogen Sorption Properties. *J. Am. Chem. Soc.* **2010**, *132*, 2991−2997.
(27) He, L.; Liu, Y.; Liu, J.; Xiong, Y.; Zheng, J.; Liu, Y.; Tang, Z. Core−Shell Noble-Metal@Metal-Organic-Framework Nanoparticles with Highly Selective Sensing Property. *Angew. Chem., Int. Ed.* **2013**, *52*, 3741−3745.
(28) Rieter, W. J.; Taylor, K. M.; An, H.; Lin, W.; Lin, W. Nanoscale Metal-organic Frameworks as Potential Multimodal Contrast Enhancing Agents. *J. Am. Chem. Soc.* **2006**, *128*, 9024−9025.
(29) Jin, S.; Son, H.-J.; Farha, O. K.; Wiederrecht, G. P.; Hupp, J. T. Energy Transfer from Quantum Dots to Metal−organic Frameworks for Enhanced Light Harvesting. *J. Am. Chem. Soc.* **2013**, *135*, 955−958.
(30) Jiang, H.-L.; Liu, B.; Akita, T.; Haruta, M.; Sakurai, H.; Xu, Q. Au@ ZIF-8: CO Oxidation over Gold Nanoparticles Deposited to Metal−organic Framework. *J. Am. Chem. Soc.* **2009**, *131*, 11302−11303.
(31) Ameloot, R.; Roeffaers, M. B.; De Cremer, G.; Vermoortele, F.; Hofkens, J.; Sels, B. F.; De Vos, D. E. Metal−organic Framework Single Crystals as Photoactive Matrices for the Generation of Metallic Microstructures. *Adv. Mater.* **2011**, *23*, 1788−1791.
(32) Falcaro, P.; Hill, A. J.; Nairn, K. M.; Jasieniak, J.; Mardel, J. I.; Bastow, T. J.; Mayo, S. C.; Gimona, M.; Gomez, D.; Whitfield, H. J. A New Method to Position and Functionalize Metal-organic Framework Crystals. *Nat. Commun.* **2011**, *2*, 237−244.
(33) Sugikawa, K.; Furukawa, Y.; Sada, K. SERS-active Metal−organic Frameworks Embedding Gold Nanorods. *Chem. Mater.* **2011**, *23*, 3132−3134.
(34) Lu, G.; Li, S.; Guo, Z.; Farha, O. K.; Hauser, B. G.; Qi, X.; Wang, Y.; Wang, X.; Han, S.; Liu, X. Imparting Functionality to a Metal−organic Framework Material by Controlled Nanoparticle Encapsulation. *Nat. Chem.* **2012**, *4*, 310−316.
(35) Zhang, Z.; Chen, Y.; Xu, X.; Zhang, J.; Xiang, G.; He, W.; Wang, X. Well-Defined Metal−Organic Framework Hollow Nanocages. *Angew. Chem.* **2014**, *126*, 439−443.
(36) Corma, A.; Iglesias, M.; Llabrés i Xamena, F. X.; Sánchez, F. Cu and Au Metal−organic Frameworks Bridge the Gap between Homogeneous and Heterogeneous Catalysts for Alkene Cyclopropanation Reactions. *Chem.—Eur. J.* **2010**, *16*, 9789−9795.
(37) Llabrés i Xamena, F. X.; Abad, A.; Corma, A.; Garcia, H. MOFs as Catalysts: Activity, Reusability and Shape-selectivity of a Pd-containing MOF. *J. Catal.* **2007**, *250*, 294−298.
(38) Wang, Y.; Zhong, H.; Hu, L.; Yan, N.; Hu, H.; Chen, Q. Manganese Hexacyanoferrate/MnO_2 Composite Nanostructures as a Cathode Material for Supercapacitors. *J. Mater. Chem. A* **2013**, *1*, 2621−2630.
(39) Chiang, Y. D.; Hu, M.; Kamachi, Y.; Ishihara, S.; Takai, K.; Tsujimoto, Y.; Ariga, K.; Wu, K. C. W.; Yamauchi, Y. Rational Design and Synthesis of Cyano-Bridged Coordination Polymers with Precise Control of Particle Size from 20 to 500 nm. *Eur. J. Inorg. Chem.* **2013**, *2013*, 3141−3145.
(40) Ming, H.; Torad, N. L.; Chiang, Y.-D.; Wu, K. C.-W.; Yamauchi, Y. Size- and Shape-controlled Synthesis of Prussian Blue Nanoparticles by a Polyvinylpyrrolidone-assisted Crystallization Process. *CrystEngComm* **2012**, *14*, 3387−3396.
(41) Shieh, F. K.; Wang, S. C.; Leo, S. Y.; Wu, K. C. W. Water-Based Synthesis of Zeolitic Imidazolate Framework-90 (ZIF-90) with a Controllable Particle Size. *Chem.—Eur. J.* **2013**, *19*, 11139−11142.
(42) Chen, C.; Kang, Y.; Huo, Z.; Zhu, Z.; Huang, W.; Xin, H. L.; Snyder, J. D.; Li, D.; Herron, J. A.; Mavrikakis, M. Highly Crystalline Multimetallic Nanoframes with Three-dimensional Electrocatalytic Surfaces. *Science* **2014**, *343*, 1339−1343.
(43) Tauster, S.; Fung, S.; Baker, R.; Horsley, J. Strong Interactions in Supported-metal Catalysts. *Science* **1981**, *211*, 1121−1125.
(44) Hickman, A. J.; Sanford, M. S. High-valent Organometallic Copper and Palladium in Catalysis. *Nature* **2012**, *484*, 177−185.
(45) Liang, H. P.; Zhang, H. M.; Hu, J. S.; Guo, Y. G.; Wan, L. J.; Bai, C. L. Pt Hollow Nanospheres: Facile Synthesis and Enhanced Electrocatalysts. *Angew. Chem.* **2004**, *116*, 1566−1569.
(46) Macdonald, J. E.; Sadan, M. B.; Houben, L.; Popov, I.; Banin, U. Hybrid Nanoscale Inorganic Cages. *Nat. Mater.* **2010**, *9*, 810−815.
(47) Oh, M. H.; Yu, T.; Yu, S.-H.; Lim, B.; Ko, K.-T.; Willinger, M.-G.; Seo, D.-H.; Kim, B. H.; Cho, M. G.; Park, J.-H. Galvanic Replacement Reactions in Metal Oxide Nanocrystals. *Science* **2013**, *340*, 964−968.
(48) Penn, R. L. Kinetics of oriented aggregation. *J. Phys. Chem. B* **2004**, *108*, 12707−12712.
(49) Wang, Y.; Chen, Q. Dual-layer Structured Nickel Hexacyanoferrate/MnO_2 Composite as a High-energy Super-capacitive Material Based on the Complementarity and Interlayer Concentration Enhancement Effect. *ACS Appl. Mater. Interfaces* **2014**, *6*, 6196−6201.
(50) Behrens, S.; Heyman, A.; Maul, R.; Essig, S.; Steigerwald, S.; Quintilla, A.; Wenzel, W.; Bürck, J.; Dgany, O.; Shoseyov, O. Constrained Synthesis and Organization of Catalytically Active Metal Nanoparticles by Self-Assembled Protein Templates. *Adv. Mater.* **2009**, *21*, 3515−3519.
(51) Bond, G. C. The Origins of Particle Size Effects in Heterogeneous Catalysis. *Surf. Sci.* **1985**, *156*, 966−981.
(52) Strizhak, P. Nanosize Effects in Heterogeneous Catalysis. *Theor. Exp. Chem.* **2013**, *49*, 2−21.
(53) Mayrhofer, K.; Blizanac, B.; Arenz, M.; Stamenkovic, V.; Ross, P.; Markovic, N. The Impact of Geometric and Surface Electronic Properties of Pt-catalysts on the Particle Size Effect in Electrocatalysis. *J. Phys. Chem. B* **2005**, *109*, 14433−14440.
(54) Zhang, P.; Li, R.; Huang, Y.; Chen, Q. A Novel Approach for the in Situ Synthesis of Pt−Pd Nanoalloys Supported on Fe_3O_4@C Core−Shell Nanoparticles with Enhanced Catalytic Activity for Reduction Reactions. *ACS Appl. Mater. Interfaces* **2014**, *6*, 2671−2678.
(55) Wunder, S.; Polzer, F.; Lu, Y.; Mei, Y.; Ballauff, M. Kinetic Analysis of Catalytic Reduction of 4-nitrophenol by Metallic Nanoparticles Immobilized in Spherical Polyelectrolyte Brushes. *J. Phys. Chem. C* **2010**, *114*, 8814−8820.
(56) Xu, W.; Kong, J. S.; Yeh, Y.-T. E.; Chen, P. Single-molecule Nanocatalysis Reveals Heterogeneous Reaction Pathways and Catalytic Dynamics. *Nat. Mater.* **2008**, *7*, 992−996.
(57) Mei, Y.; Lu, Y.; Polzer, F.; Ballauff, M.; Drechsler, M. Catalytic Activity of Palladium Nanoparticles Encapsulated in Spherical Polyelectrolyte Brushes and Core-shell Microgels. *Chem. Mater.* **2007**, *19*, 1062−1069.
(58) Kong, X.-k.; Sun, Z.-y.; Chen, M.; Chen, Q.-w. Metal-free Catalytic Reduction of 4-nitrophenol to 4-aminophenol by N-doped Grapheme. *Energy Environ. Sci.* **2013**, *6*, 3260−3266.
(59) Liu, X. Heterogeneous Nucleation or Homogeneous Nucleation? *J. Chem. Phys.* **2000**, *112*, 9949−9955.
(60) Kaye, S. S.; Long, J. R. Hydrogen Storage in the Dehydrated Prussian Blue Analogues $M_3[Co(CN)_6]_2$ (M= Mn, Fe, Co, Ni, Cu, Zn). *J. Am. Chem. Soc.* **2005**, *127*, 6506−6507.
(61) Chapman, K. W.; Southon, P. D.; Weeks, C. L.; Kepert, C. J. Reversible Hydrogen Gas Uptake in Nanoporous Prussian Blue Analogues. *Chem. Commun.* **2005**, 3322−3324.

DOI: 10.1021/am508246m
ACS Appl. Mater. Interfaces 2015, 7, 2088−2096

(62) Proch, S.; Herrmannsdörfer, J.; Kempe, R.; Kern, C.; Jess, A.; Seyfarth, L.; Senker, J. Pt@MOF-177: Synthesis, Room-Temperature Hydrogen Storage and Oxidation Catalysis. *Chem.—Eur. J.* **2008**, *14*, 8204−8212.

DOI: 10.1021/am508246m
ACS Appl. Mater. Interfaces 2015, 7, 2088−2096